1 Survey of Experiments

A survey of key experiments exhibiting the quantum phases of matter studied in this book. Experiments on metals, band insulators, magnetic order and spin liquids in Mott insulators, ultracold atoms, the heavy fermion compounds, and the cuprate superconductors are described.

The theory of electronic quantum matter began in 1928, soon after the formulation of quantum mechanics, when Sommerfeld [265] proposed a theory of metals, using independent electrons obeying Fermi–Dirac statistics. Many experimental and theoretical developments followed, leading to a very successful theory of metals, semiconductors, superconductors, and insulators. This theory accounted for the Coulomb interactions between the electrons, but nevertheless the independent-electron paradigm survived in the form of a theory of nearly-independent electronic quasiparticles with the same spin and charge as an electron.

Beginning in the early 1980s, observations on new "quantum materials" could not be easily fit into such an independent-electron paradigm, and this stimulated the development of new theories of quantum matter in which the many-particle wavefunction is fundamentally different from a product of single-particle states, that is, the particles are "entangled." Many of these theoretical developments are described in this book, beginning in Part II. In this chapter, I present a selective survey of some experimental observations that motivated these studies. There is no attempt at completeness here, this is just a selection of experiments that highlight the main phenomena.

1.1 Metals and Band Insulators

In the independent-electron theory, the electrons occupy states in Bloch bands specified by a crystal momentum $\boldsymbol{k}$ and a band index n (which we will often drop because of our focus on single-band models). The values of $\boldsymbol{k}$ extend over the first Brillouin zone of the lattice. By considering a finite lattice, most conveniently with periodic boundary conditions, we can discretize the values of $\boldsymbol{k}$ and count the number of $\boldsymbol{k}$ states: the total number of $\boldsymbol{k}$ states in the first Brillouin zone equals the total number of unit cells in the finite lattice. Consequently, the density of electrons in a fully filled band is one per unit cell and per spin. A crystal with an odd number of electrons per unit cell, and

https://doi.org/10.1017/9781009212717.002 Published online by Cambridge University Press

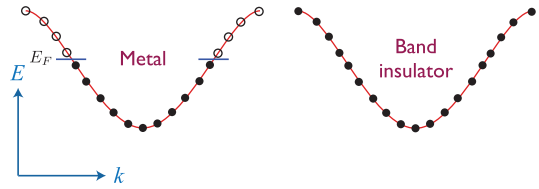

Figure 1.1 Electrons occupying states in a Bloch band. Each filled circle represents two electrons, after accounting for the spin degeneracy. A metal has a partially filled band, and this allows for excitations with vanishing energy near the Fermi surface separating the occupied and empty states. The Fermi energy is $E_{\rm F}$.

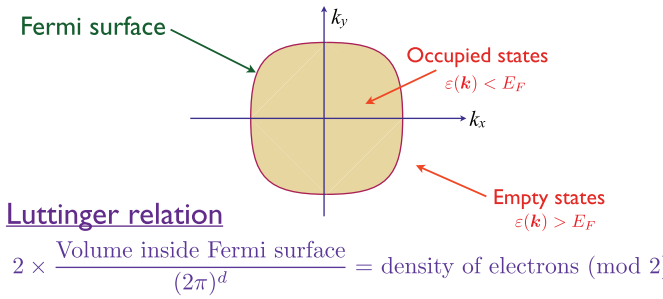

Figure 1.2 The Fermi surface and the Luttinger relation of Fermi liquid theory. The modulo 2 (mod 2) accounts for the electrons in fully filled bands, and assumes that electron spins are unpolarized.

with spin unpolarized, cannot fully fill a Bloch band, and so must be a metal in the independent-electron theory – this is illustrated in Fig. 1.1.

When there are an even number of electrons per unit cell, then a band insulator is a possible outcome, as also shown in Fig. 1.1. All bands in a band insulator are either completely empty or fully occupied. There is an energy gap towards creating excitations, which require moving an electron from a filled band to an empty band. However, when there is overlap in the energy eigenvalues of different bands with different $\boldsymbol{k}$ values, we can have multiple bands partially filled, and so a metal is another possible outcome with an even number of electrons per unit cell.

Going beyond the independent-electron theory, interactions in a metal can be accounted for in the context of Fermi liquid theory, as discussed in Chapter 2. The independent-electron theory of a metal implies the existence of a Fermi surface in $\boldsymbol{k}$ space, which separates the occupied and empty states of a partially filled band, as shown in Fig 1.2. The concept of a Fermi surface withstands the presence of interactions, and its position remains precisely defined in a Fermi liquid. A crucial result of Fermi liquid theory is that the volume enclosed by the Fermi surface does not change as the interactions are turned on – we prove this Luttinger relation in Section 30.2. Indeed, the concept of a Fermi surface is remarkably robust, and even holds in metallic states without quasiparticle excitations, as discussed in Chapter 34.

https://doi.org/10.1017/9781009212717.002 Published online by Cambridge University Press

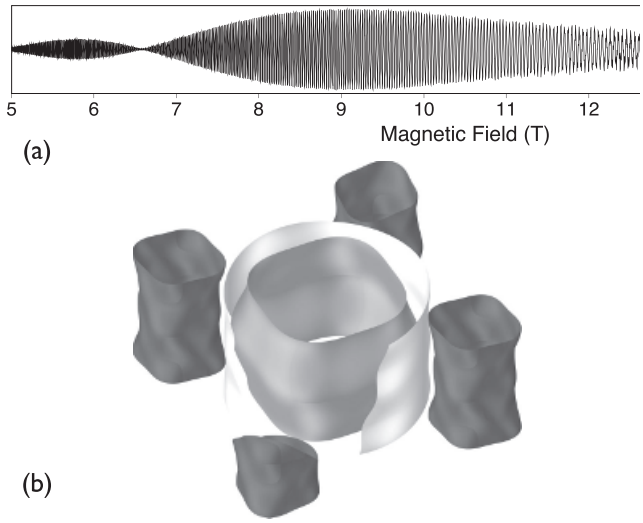

Figure 1.3 (a) Oscillations in the magnetization (dHvA oscillations) of Sr_2RuO_4 in a magnetic field. Such data are used to construct the multiple sheets of the Fermi surface shown in (b) is a quasi-two-dimensional material and the ripples in the vertical direction have been exaggerated by a factor of 15. From Ref. [26]. Reprinted with permission from APS.

The presence of a Fermi surface in a metal and the associated low-energy excitations across the Fermi surface dominate the observable properties of a metal. Among the consequences of a Fermi surface are

- The entropy S and the specific heat C of a metal vanish as temperature $T \to 0$ as

$$S = C = N\gamma T\,, \tag{1.1}$$

  where N is the total number of electrons. The Sommerfeld coefficient γ is proportional to the density of quasiparticle states at the Fermi level.
- The response to an applied magnetic field with a Zeeman coupling to the electrons is given by the Pauli spin susceptibility $\chi(T \to 0) = \chi_0$, where χ_0 is also proportional to the quasiparticle density of states at the Fermi level.
- In the presence of impurities, the resistivity ρ of a metal has the T dependence,

$$\rho(T) = \rho_0 + AT^2\,, \tag{1.2}$$

  where the A coefficient is controlled by the quasiparticle interactions.

The presence of a Fermi surface also induces oscillations in various observables in the presence of an applied magnetic field, as shown in Fig. 1.3. Such oscillations can be used to deduce remarkably precise information on the shape of the Fermi surface.

https://doi.org/10.1017/9781009212717.002 Published online by Cambridge University Press

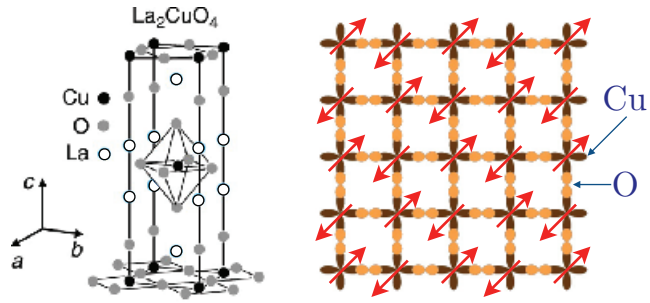

Figure 1.4 The Mott insulator La_2CuO_4. The active band resides on CuO_2 planes. At low T, there is broken lattice and spin rotation symmetry, with the electrons forming the Néel state, with a non-zero staggered magnetic moment centered on each Cu site.

1.2 Mott Insulators

The precise definition of a Mott insulator is a bit ambiguous in the literature. But, generally speaking, a Mott insulator is a crystal which is an insulator even though band theory requires the crystal to be a metal. Specifically, band theory requires a spin-unpolarized system with an odd number of electrons per unit cell to be a metal, as we noted above. Nevertheless, electron–electron interactions can drive such a system to be an insulator. The ambiguity arises when electron–electron interactions also induce some form of lattice symmetry breaking at low temperatures, and the size of the unit cell is at least doubled, so that there are now an even number of electrons in the new unit cell. Then, strictly speaking, band theory would allow the formation of a band insulator. Nevertheless, we will follow common practice, and continue to label such an insulator a Mott insulator. The influence of electron–electron interactions is paramount in such an insulator, as the energy gap to charged excitations is usually much larger than the energy gap that is deduced from a band-theory analysis.

The best-studied Mott insulator is the compound La_2CuO_4, shown in Fig. 1.4. The great interest is largely due to the appearance of high-temperature superconductivity when this compound is doped, as discussed below. We can describe the low-energy properties of this material by a single-band model with the orbitals centered on the Cu atoms on the vertices of a square lattice. In the insulator, this band has one electron per unit cell of the square lattice, and so band theory predicts this material must be a metal. However, electron–electron interactions, dominated by an on-site repulsion U between two opposite-spin electrons, make this system an insulator. The single-band model with interaction U is the Hubbard model, which is discussed further in Chapter 9.

At low T, the unit cell in La_2CuO_4 is doubled by the onset of Néel order shown in Fig. 1.4. Now there are two electrons per unit cell, and so the Néel state are allowed to be an insulator by band theory. In other words, we can adiabatically connect the Néel state to an insulator in the small U limit, provided we maintain the broken symmetry of the Néel state. However, the energy scales of excitations in the large U Néel state are

https://doi.org/10.1017/9781009212717.002 Published online by Cambridge University Press

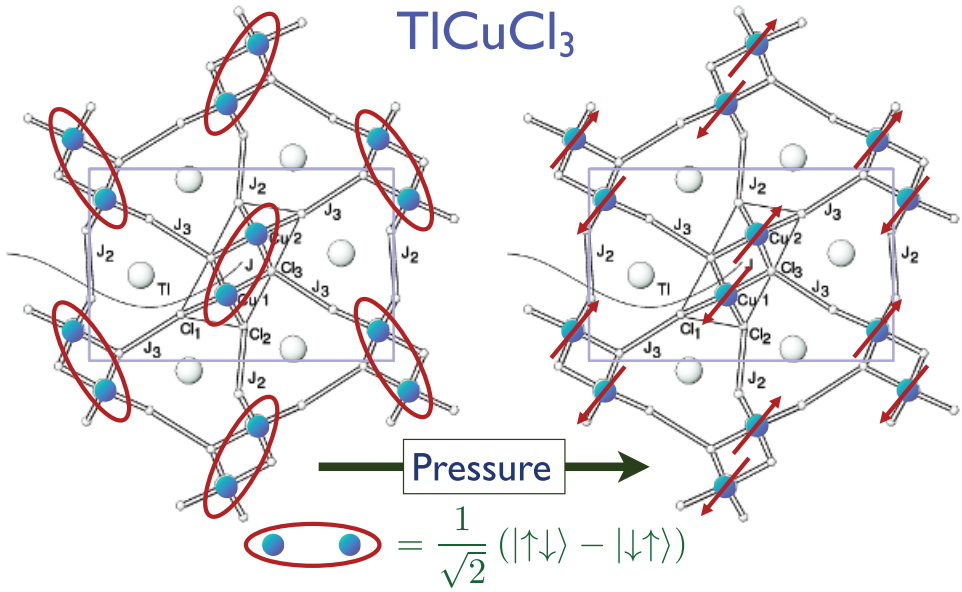

Figure 1.5 $TlCuCl_3$ under ambient pressure is an insulator with a spin gap, with electrons on Cu sites paired into spin singlets (left). Applying pressure induces a quantum phase transition to a Néel state with broken spin rotation symmetry.

very different from the small U band insulator with Néel order, which is why we prefer to label the large U state a Mott insulator. Specifically, the charge gap in the large U case is of order U, and is independent of the strength of the Néel order; in contrast, the charge gap in the band insulator is determined by the strength of the magnetic Néel order.

Another interesting insulator is $TlCuCl_3$, shown in Fig. 1.5. This insulator has one unpaired electron on each Cu atom, and an even number of Cu atoms per unit cell. Consequently, it can be adiabatically connected to a band insulator. However, it is better to think of it as a Mott insulator, in which the electrons on the Cu sites remain immobile, and pair up into spin singlets between neighboring Cu atoms, as shown in the left panel of Fig. 1.5. Note that the pairing pattern preserves all the symmetries of the crystal structure. Upon applying pressure, a quantum phase transition is observed at a critical pressure, above which the ground state becomes a Néel state, similar to that found in La_2CuO_4. The spins are now polarized in a staggered pattern, as shown in the right panel of Fig. 1.5.

The theory for the quantum phase transition in $TlCuCl_3$ is reviewed in Section 11.2. It is a relativistic field theory for the Néel order parameter in $3+1$ dimensions (the configuration of Cu atoms is three-dimensional in $TlCuCl_3$, unlike the two-dimensionality of La_2CuO_4). Section 11.2 also describes the evolution of the excitation spectrum across the quantum phase transition, and such a spectrum has been measured by neutron scattering, as shown in Fig. 1.6.

Another example of a pressure-induced transition from a gapped quantum paramagnet to a Néel state appears in the compound $SrCu_2(BO_3)_2$ [323], and is shown in

https://doi.org/10.1017/9781009212717.002 Published online by Cambridge University Press

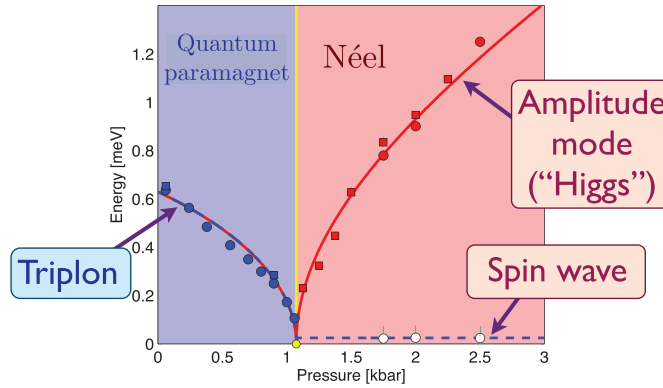

Figure 1.6 Neutron scattering observations [225] across the pressure-induced quantum phase transition in $TlCuCl_3$. The triplon particle is a spin-triplet excitation on a pair of Cu sites, which hops on the pairs shown on the left in Fig. 1.5; a field-theoretic description of this excitation is in Section 11.2.1. The spin-wave and amplitude-mode excitations of the Néel state are described in Section 11.2.3. Reprinted with permission from APS.

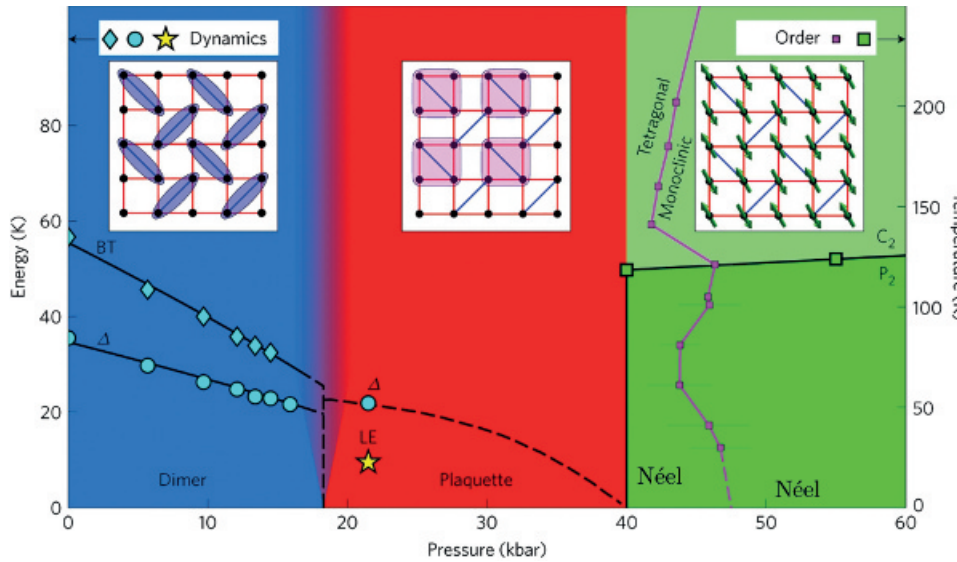

Figure 1.7 Phase diagram of $SrCu_2(BO_3)_2$ under pressure [323]. The dimer phase breaks no symmetries of the lattice, while the Néel phase breaks spin rotation symmetry. The intermediate plaquette phase is a VBS, and it breaks lattice symmetries while preserving spin rotation symmetry. Reprinted with permission from Springer Nature.

Fig. 1.7. At ambient pressure, this compound is a gapped quantum paramagnet in which the spins on the Cu sites form singlet pairs in a manner that does not break any lattice symmetries, just as in $TlCuCl_3$. At large pressure there is a collinear Néel state, which breaks spin rotation symmetry, also as in $TlCuCl_3$. The new phenomenon here is

https://doi.org/10.1017/9781009212717.002 Published online by Cambridge University Press

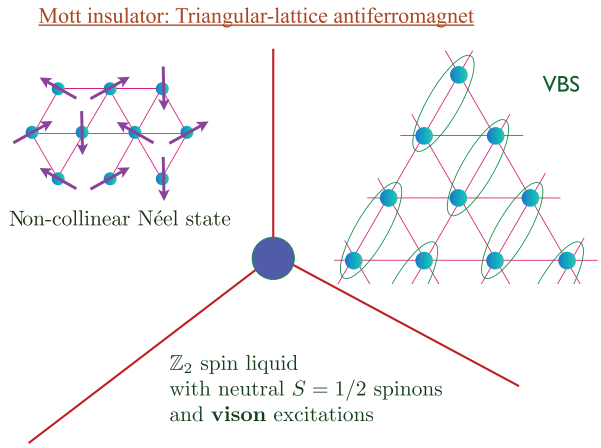

Figure 1.8 Schematic of possible phases of systems with $S = 1/2$ spins on the sites of a triangular lattice, and coupled with antiferromagnetic exchange interactions. The transition between the $\mathbb{Z}_2$ spin liquid and the non-collinear Néel state is discussed in Section 15.4.1, near Fig. 15.5. The transition between the $\mathbb{Z}_2$ spin liquid and VBS is discussed in Sections 16.5.2 and 26.2.3, and Chapter 28. The transition from the VBS to the non-collinear Néel state is discussed in Refs. [120, 268, 270].

the intermediate plaquette valence-bond solid (VBS) phase, in which four spins in a plaquette form a spin singlet, and the choice of the four-spin plaquettes requires a breaking of lattice symmetry. I discuss such collinear Néel–VBS quantum phase transitions in Chapter 28.

We turn now to insulators in which the immobile electrons reside on triangular or kagome lattices. Some possible fates of the electronic spins are sketched in Fig. 1.8. If the exchange interactions between the spins are antiferromagnetic, then such lattices are "frustrated," because it is not possible to find classical spin configurations in which the energy of each bond is minimized. The classical antiferromagnet has non-collinear Néel order, as shown in Fig. 1.8. Such Néel states can also be found for quantum $S = 1/2$ spins, and have been observed in $Ba_3CoSb_2O_9$ [166], as shown in Fig. 1.9.

Another state in Fig. 1.8 is the VBS. The spins pair into spin-singlet bonds as in the gapped state of $TlCuCl_3$. But this pairing breaks the symmetry of the triangular lattice, and there are six equivalent patterns of the columnar pattern of singlet bonds; this is similar to the plaquette VBS state of $SrCu_2(BO_3)_2$. This symmetry breaking has important consequences for the quantum phase transitions out of the VBS phase, as investigated in Sections 16.5.2 and 26.2.3, and Chapter 28. An example of a VBS state in κ-(BEDT-TTF)$_2$Cu$_2$(CN)$_3$ [178] is shown in Fig. 1.10.

The remaining phase in Fig. 1.8 is the $\mathbb{Z}_2$ spin liquid. This does not break any symmetries, either lattice or spin rotation. So this state is a true Mott insulator, with no caveats. It realizes a resonating valence-bond spin liquid, and will be the focus of much discussion starting in Chapter 13. There is "long-range quantum entanglement" in a spin liquid, and so it cannot be studied by the traditional perturbative approaches of

https://doi.org/10.1017/9781009212717.002 Published online by Cambridge University Press

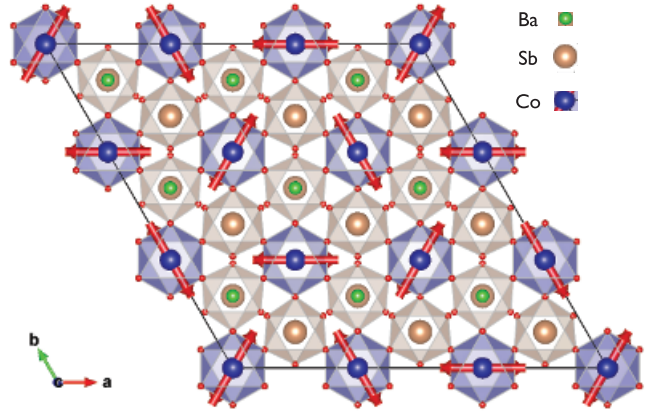

Figure 1.9 Non-collinear Néel order of $Ba_3CoSb_2O_9$ [166]. The arrows indicate the direction of the magnetic moment on the Co sites.

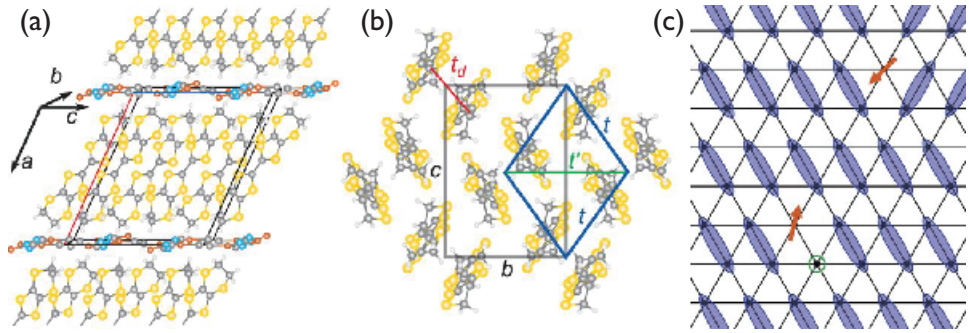

Figure 1.10 A valence bond solid state in the organic compound κ-(BEDT-TTF)$_2$Cu$_2$(CN)$_3$ shown in (a) [178]. There is a single unpaired spin on each organic molecule, and the molecules reside on a distorted triangular lattice distorted triangular lattice shown in (b). These spins pair up to form the valence bond solid shown in (c). Reprinted with permission from AAAS.

quantum many-body theory to be reviewed in Part I. As an experimental example, note the observations [77] on $Cu_3Zn(OH)_6FBr$ in Fig. 1.11, in which the spins reside on the Cu atoms on a kagome lattice.

1.3 Ultracold Atoms

While the focus of this book is on electronic quantum matter, we will also consider studies of ultracold atoms. Remarkable advances in cooling and trapping atoms have opened in a new frontier in the experimental study of quantum many-body systems. These offer a new set of experimental tools to study novel quantum phases, often with single-site resolution, and the ability to control the couplings in the Hamiltonian.

https://doi.org/10.1017/9781009212717.002 Published online by Cambridge University Press

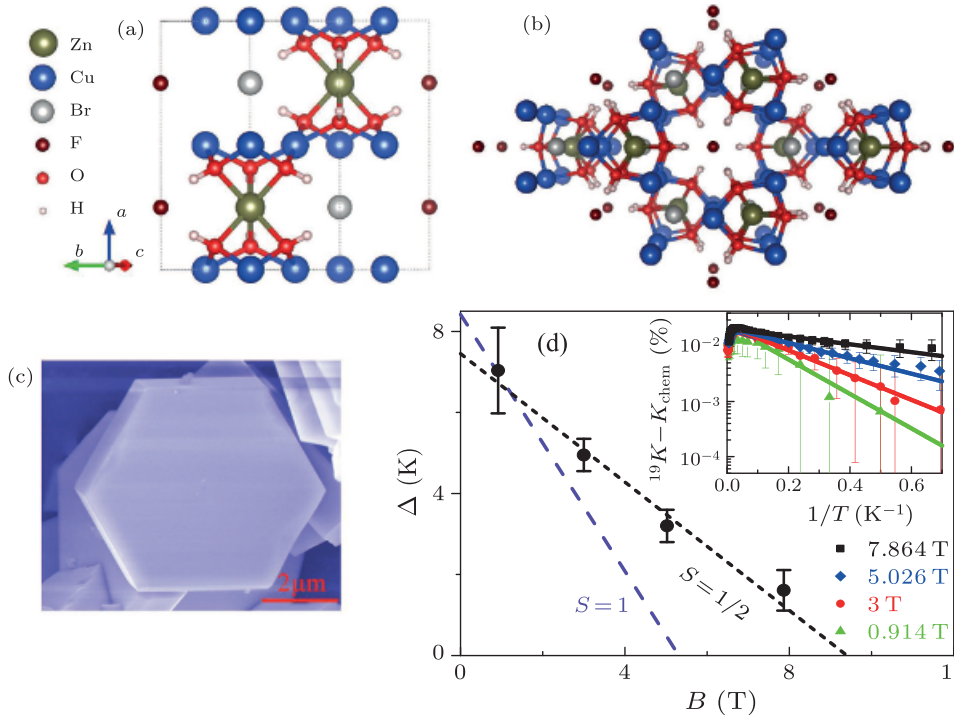

Figure 1.11 (a) and (b) Crystal structures of the gapped spin liquid candidate $Cu_3Zn(OH)_6FBr$ [77]. An image of a crystal is shown in (c). (d) The spin gap Δ is measured in an applied magnetic field, and its slope indicates the presence of fractionalized spin $S = 1/2$ excitations. Reprinted with permission from *Chinese Physics Letters*.

Connecting such studies to those in electronic quantum matter is a promising avenue for future research.

The first studies of ultracold atoms focused on bosonic atoms, and cooling them to a superfluid state: the theory of the dilute Bose gas is presented Chapter 3. Subsequently, the atoms were placed in a periodic potential, and the superfluid–insulator quantum phase transition was observed [95] as shown in Fig. 1.12. This is a Mott insulator, because of repulsive interactions between the bosons, and an integer density of bosons per unit cell. The transition of bosons between a Mott insulator and a superfluid are discussed in Chapter 8.

More recent experiments have also examined Mott insulators of spin-1/2 fermionic atoms, which form a Néel state on the square lattice, similar to La_2CuO_4 in Fig. 1.4. By varying the density of atoms, these studies have now explored the phase diagram of the doped Mott insulator. This is similar to the doped cuprate compounds, which are discussed in Section 1.5. However the accessible temperatures in the ultracold-atom systems are rather high on the relevant microscopic energy scales, in comparison to the cuprates. Superconductivity has not yet been observed, but new information has been revealed on the microscopic correlations at higher temperatures, as shown

https://doi.org/10.1017/9781009212717.002 Published online by Cambridge University Press

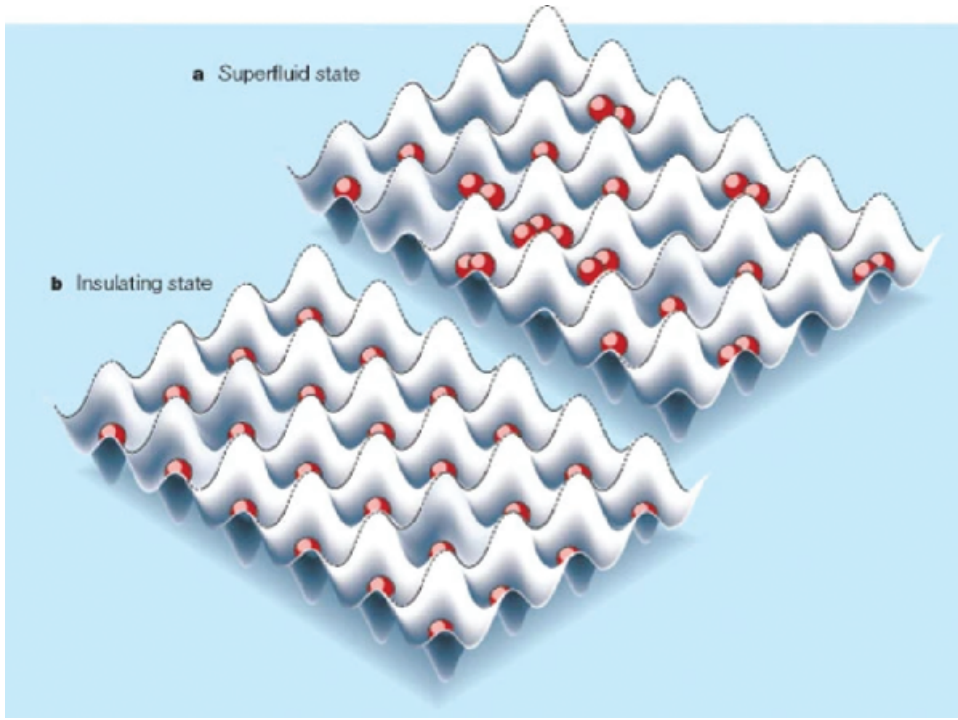

Figure 1.12 The superfluid–insulator transition of ultracold, bosonic, Rb atoms [95, 276]. Reprinted with permission from Springer Nature.

in Fig. 1.13. We will begin our study of the fermionic doped Mott insulators in Chapter 9, with a focus on the low-temperature superfluidity. This superfluidity is believed to be in the same class as the Bardeen–Cooper–Schrieffer (BCS) theory of the condensation of fermion pairs, which is described in Chapter 4. At higher temperatures, the fermionic doped Mott insulators exhibit the "pseudogap metal" and the "strange metal," as shown in Fig. 1.13: these are phases of matter which acquire non-trivial many-body correlations, similar to those of spin liquids. A theory of the pseudogap metal is described in Section 31.4, and that of the strange metal in Chapter 34.

A different class of ultracold-atom experiments trap atoms in laser tweezers, as shown in Fig. 1.14. A separate laser excites the atoms into Rydberg states, which have a much larger size, and have large repulsive interactions with neighboring atoms excited to Rydberg states. This off-site interaction induces quantum correlations between the different Rydberg atoms, and this leads to rich possibilities for novel correlated phases. Figure 1.15 shows theoretical predictions [244] for the phases of Rydberg atoms on a square lattice. The phases are distinguished by the wavevectors of modulations in the density of Rydberg excited states, which are absent only in the "disordered" regime. Unlike the optical lattice experiments in Fig. 1.12, there is no superfluid phase here because the number of atoms in the Rydberg states are not conserved. Experiments on

https://doi.org/10.1017/9781009212717.002 Published online by Cambridge University Press

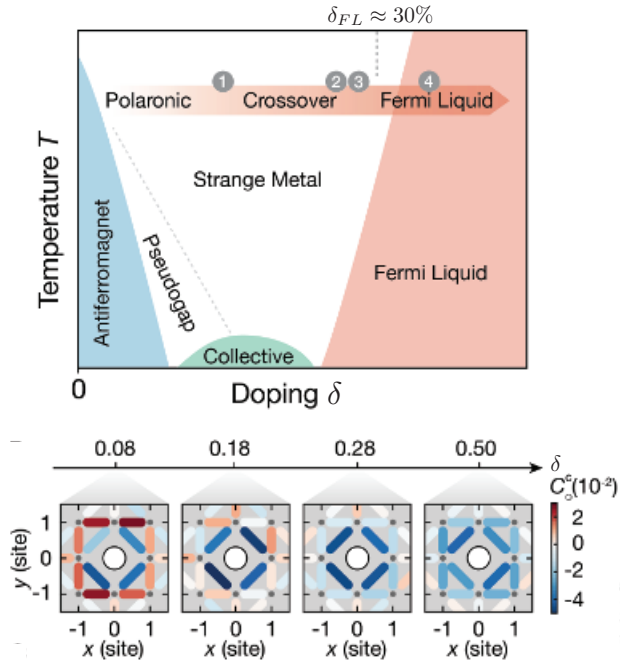

Figure 1.13 Phase diagram of the doped Mott insulator realized by ultracold fermionic atoms on a square lattice [145]. The experiments have explored spin correlations at high temperatures as a function of the doping δ. The bottom panel sketches the evolution in the spin correlations around a mobile hole with increasing δ. Reprinted with permission from AAAS.

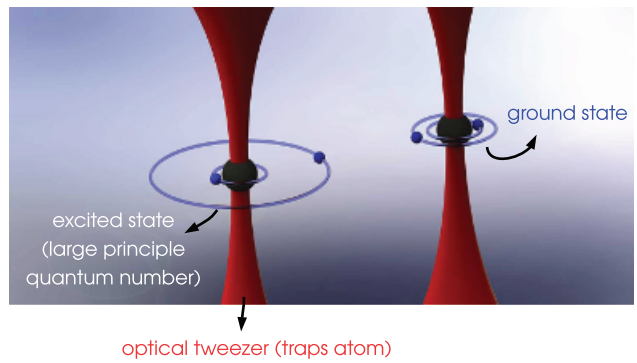

Figure 1.14 Atoms trapped by laser tweezers. The atoms can be excited to a Rydberg state by separate lasers. Figure by Jacob P. Covey.

square-lattice arrays [65] are in close correspondence with the theoretical predictions, and have also explored the quantum phase transitions between the states.

A more recent experiment [254] using Rydberg atoms studied Rydberg atoms arranged on the links of a kagome lattice, as shown in Fig. 1.16. This experiment

https://doi.org/10.1017/9781009212717.002 Published online by Cambridge University Press

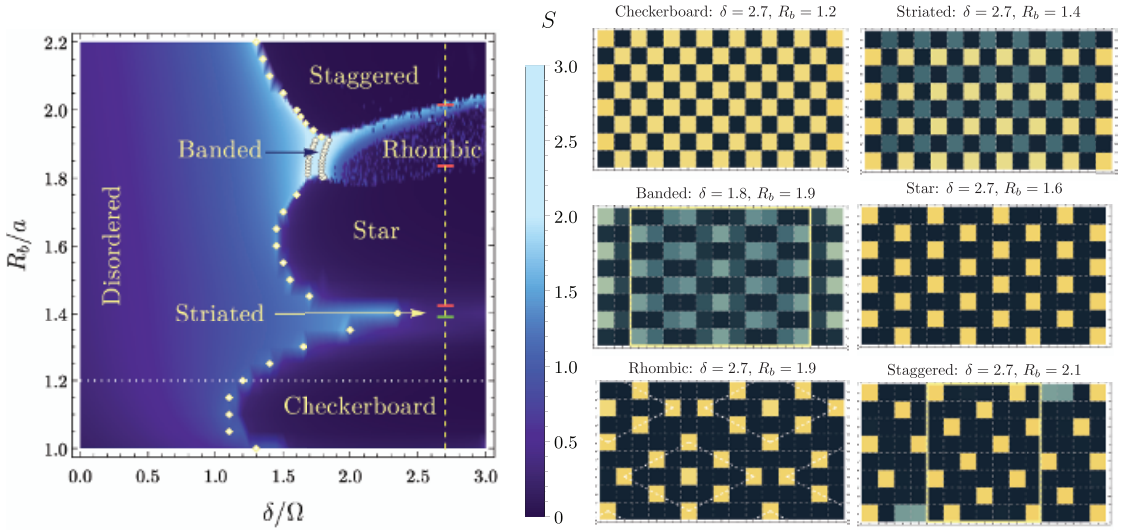

Figure 1.15 Density-matrix renormalization group results [244] for the phases of a square-lattice array of Rb atoms in laser tweezers shown in Fig. 1.14. The lattice spacing is a, the Rydberg blockade radius is R_b, the laser detuning is δ, and the Rabi frequency for the ground state to Rydberg state transition is Ω. Reprinted with permission from APS.

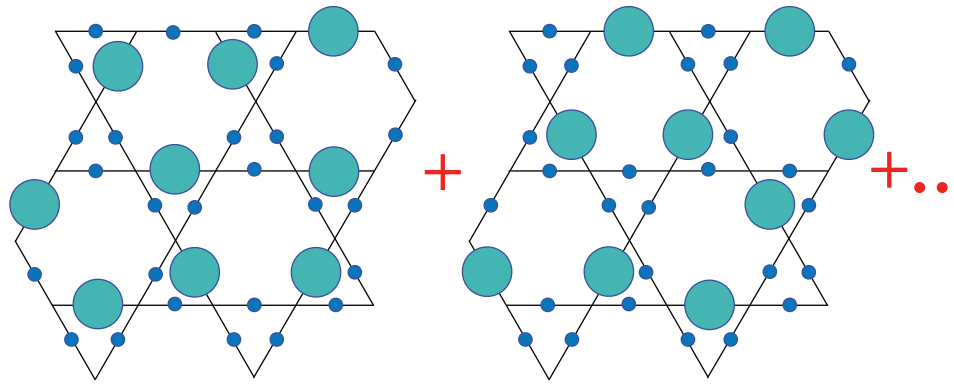

Figure 1.16 A quantum liquid of excited Rydberg atoms (indicated by the larger circles), along with atoms in the ground state (indicated by the smaller circles). The state is a coherent superposition of many such configurations, only two of which are shown above.

shows evidence for the quantum correlations of a "spin liquid" state that is discussed in Section 16.6. Similar to the spin liquid noted in Fig. 1.11, this is a state which is the coherent superposition of many configurations of atoms excited into the larger Rydberg state. The excitations "resonate" with each other, similar to the resonating-valence-bond state to be discussed starting in Chapter 13.

https://doi.org/10.1017/9781009212717.002 Published online by Cambridge University Press

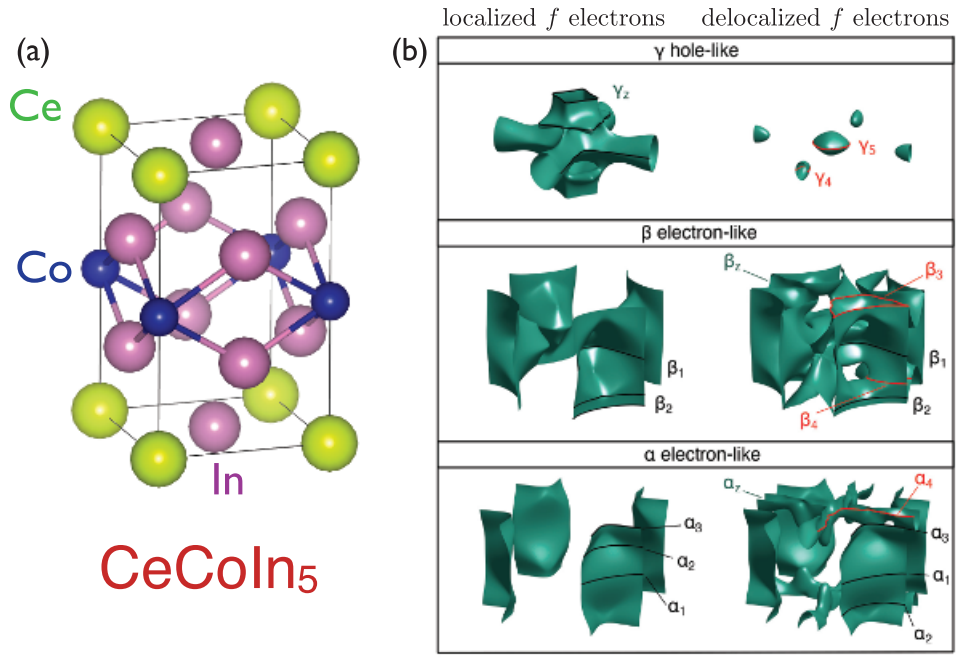

Figure 1.17 (a) Crystal structure of $CeCoIn_5$. (b) Fermi surfaces of $CeCoIn_5$ as measure by quantum oscillations [169]. In pure $CeCoIn_5$, the Fermi surfaces are computed by a theory which assumes the f electron on Ce is localized and not part of the Fermi surface. After doping with 0.33% Sn, the Fermi surface includes the f electron, which has now become mobile. Reprinted with permission from AAAS.

1.4 The Heavy-Fermion Intermetallic Compounds

Finally we turn to metallic electronic states with strong correlations, distinct from the metallic Fermi liquid states discussed in Section 1.1. The heavy-fermion compounds are described by Kondo lattice models, which are discussed in Chapter 30.

An example of such a compound is $CeCoIn_5$, shown in Fig. 1.17. The rare-earth element Ce has an electron in the f band which is nearly localized on the atomic site. However, the spin of this f electron is an active degree of freedom, which interacts via an exchange coupling with the mobile electrons from the other bands: this leads to a description as a Kondo lattice model. At generic electron densities, the ground state of the Kondo lattice model is a metal. A key question is whether this metal is in the class of Fermi liquid states discussed in Fig. 1.2. Such a state must obey the Luttinger relation, which dictates that the f states must also be included in the count of states contributing to the volume of the Fermi surface. And indeed many intermetallic compounds realize such a "heavy Fermi liquid" state, in which the main consequence

https://doi.org/10.1017/9781009212717.002 Published online by Cambridge University Press

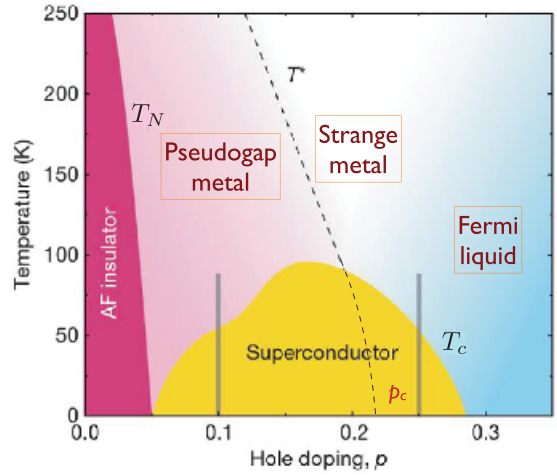

Figure 1.18 Schematic phase diagram of the hole-doped cuprate superconductors. The $p = 0$ line is a Mott insulator with antiferromagnetic (AF) order, as in Fig. 1.4. Additional phases with charge-density wave order at low T are not shown.

of the nearly localized nature of the f band is that the quasiparticle excitations on the Fermi surface have a large effective mass. Such a heavy Fermi liquid state is also realized in $CeCoIn_5$ but only after doping with a small concentration of Sn – the Fermi surface of this state is shown on the right of Fig. 1.17.

But without Sn doping, $CeCoIn_5$ realizes a novel metallic state that we call the "fractionalized Fermi liquid," which is discussed in Chapter 31. In this state, the f electrons are not included in the computation of the size of the Fermi surface, and the conventional Luttinger relation is violated. Instead, the f electrons form a spin liquid, similar to that in the Mott insulator in Fig. 1.11. The absence of the f states in the Fermi volume computation implies the Fermi surface is "small" in the fractionalized Fermi liquid, in contrast to the "large" Fermi surface of the heavy Fermi liquid. The localized f-electron column in Fig. 1.17b shows the "small" Fermi surface of the fractionalized Fermi liquid state of $CeCoIn_5$.

1.5 The Cuprates

It was the discovery of the celebrated copper oxide-based high-temperature superconductors in 1987 that launched the modern era in the study of the quantum phases of matter, which is the focus of this book. The superconductivity is obtained by doping a Mott insulator, similar to La_2CuO_4 in Fig. 1.4, by changing the composition of elements away from the CuO_2 plane. The low-energy physics is described by an electronic Hubbard model, similar on the square lattice to that discussed for fermionic ultracold atoms in Fig. 1.13. A schematic phase diagram as a function of electron density $= 1 - p$ and temperature is shown in Fig. 1.18. Note the similarity to the ultracold-atom phase

https://doi.org/10.1017/9781009212717.002 Published online by Cambridge University Press

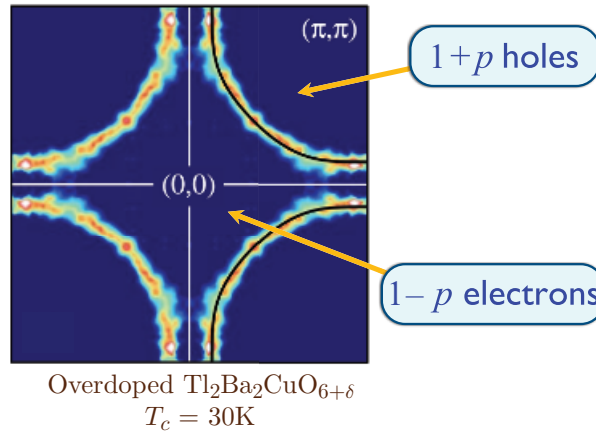

Figure 1.19 Photoemission observations [205] of the Fermi surface of in $Tl_2Ba_2CuO_{6+\delta}$ in the large-p Fermi liquid regime of Fig. 1.18. The Fermi surface obeys the conventional Luttinger relation of Fig. 1.2. Reprinted with permission from APS.

diagram in Fig. 1.13. The nature of the low-temperature phases of the antiferromagnet and superconductor is discussed in Chapter 9.

Much of Part V is directed towards a theory of the metallic phases that appear at higher temperatures, shown in Fig. 1.18 (and also in Fig. 1.13). The large-p metallic state (the "overdoped" regime) is a conventional Fermi liquid, and this is confirmed by photoemission experiments, which show a Fermi surface obeying the conventional Luttinger relation; see Fig. 1.19.

In contrast, the "pseudogap metal" at small p does not fall into the traditional Fermi liquid paradigms. A great deal of experimental effort has been devoted to carefully characterizing the remarkable properties of this pseudogap metal, and associated ordered phases at low T. I do not survey this work here, and only note the analog of the photoemission observations in Fig. 1.19, but now carried out at low T. Figure 1.20 shows that the "large Fermi surface" of Fig. 1.19 is not present at small p. Instead there is a gap in the electronic spectrum near the "antinodes" (this is the region of the Brillouin zone near $\boldsymbol{k} = (\pi, 0), (0, \pi)$). The Fermi surface appears to only be present in "arc"-like form near the "nodal region" (this is the region of the Brillouin zone near $\boldsymbol{k} = (\pm\pi/4, \pm\pi/4)$). There are strong theoretical constraints that the Fermi surface must be a closed curve, and so a natural hypothesis is that the Fermi arcs are only the front portion of small hole-pocket Fermi surfaces in the nodal region, and the photoemission intensity on the "back side" of the pockets is suppressed by a small quasiparticle residue (see Ref. [73] for transport evidence for such pocket Fermi surfaces). An attractive interpretation of such Luttinger-relation-violating small Fermi surfaces is that the pseudogap metal is a fractionalized Fermi liquid, similar to that discussed in Section 1.4 for the intermetallic compounds. However, in the cuprates there is no analog of the f band in which some of the electrons can localize and so reduce the volume enclosed by the Fermi surface. There is only one single band that crosses the Fermi level, as is amply clear from the Fermi surface observed in Fig. 1.19,

https://doi.org/10.1017/9781009212717.002 Published online by Cambridge University Press

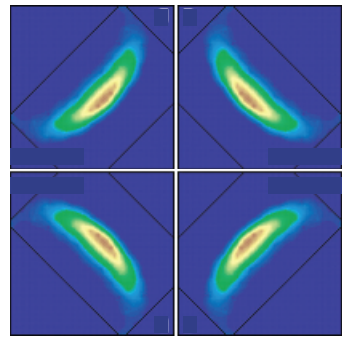

Figure 1.20 Photoemission spectrum of $Ca_{2-x}Na_xCuO_2Cl_2$ [264] in the underdoped pseudogap metal region of Fig. 1.18. Reprinted with permission from AAAS.

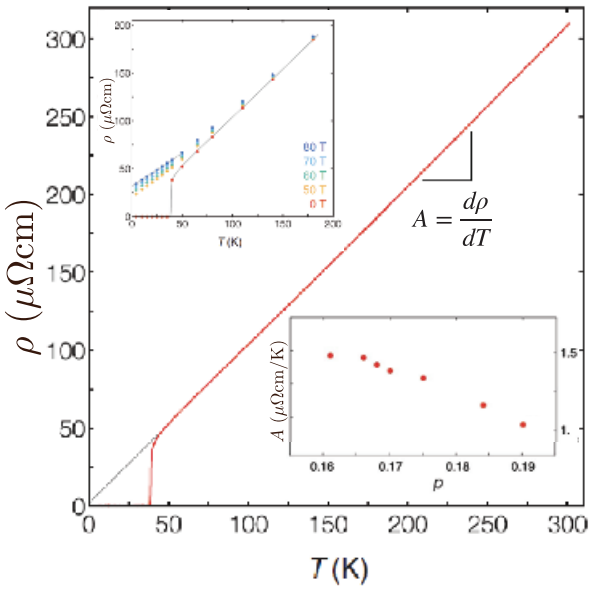

Figure 1.21 Resistivity of $La_{2-x}Sr_xCuO_4$ [94] in the strange-metal regime of Fig. 1.18. Reprinted with permission from AAAS.

and partially localizing some of the electrons in this band seems difficult to achieve. In Section 31.4 I will present a theory for the formation of a fractionalized Fermi liquid state in a single-band model: this theory is able to successfully model the photoemission spectra as a function of momentum and energy [173].

The last remaining metal in Fig. 1.18 is the "strange metal." This also does not fall into the Fermi liquid paradigm, and its well-known characteristic is the linear-in-temperature resistivity shown in Fig. 1.21. Photoemission experiments and other observations show that there are no well-defined fermionic quasiparticles in the strange

https://doi.org/10.1017/9781009212717.002 Published online by Cambridge University Press

metal, in contrast to both the pseudogap metal and the Fermi liquid. However, as discussed in Chapter 34, the breakdown of quasiparticles does not exclude the presence of a sharp Fermi surface in momentum space. In Chapter 34 I also discuss theories of strange metals without quasiparticles, along with an analysis of their transport properties.

https://doi.org/10.1017/9781009212717.002 Published online by Cambridge University Press